Preliminary Results on OCT-based Position Control of a Concentric Tube Robot

Y. Baran, K. Rabenorosoa, G. J. Laurent, P. Rougeot, N. Andreff, and B. Tamadazte

***Abstract*— This paper presents preliminary results on OCT (Optical Coherence Tomography) based control of a concentric tube robot (CTR). The potential use of OCT system is presented then its ability to perform an optical biopsy and an *eye-to-hand* configuration for robot control is highlighted. A prototype of CTR with three curved tubes is shortly described then a model-less OCT-based controller is detailed. The extraction of visual features from OCT images is performed by normalized cross-correlation. The proposed control scheme was experimentally validated. The positioning accuracy of CTR control was evaluated in benchtop trials. The error in tip placement can reach 10 μm along X and 74 μm along Y according to controller parameters. The 2D positioning (XY plan) is also tested then a final error about 55 μm is achieved.**

I. Introduction

Minimally invasive surgery (MIS) or keyhole surgery, uses small incisions, generally less than 1cm to perform intra-body procedures as compared to the larger incisions needed in the traditional open surgery techniques. During the last two decades, MIS procedures have received a growing interest in various surgery fields enabling significant technological breakthroughs in terms of surgical instruments, imaging systems, etc [1]. Among the various robotic systems for surgical assistance, especially in MIS procedures, certainly one of the most innovative and promising technology is concentric tube robot (CTR). The CTR technology is considered as a "*Swiss Army knife*" in surgery which is under numerous investigations (urology, neurosurgery, ENT surgery, cardiovascular surgery, etc.) as reviewed in [2].

Advantages of CTR have been discussed in [3] and compared to tendon-driven continuum robots [4] while design, modeling and control of CTR are widely discussed in [5], [6]. However, there remain many challenges to make these numerous possible surgical applications realistic and realizable in the operating theaters [7]. In fact, the initial research on CTR has focused on design (tube number, shape, size, etc.) [8], [9] and modeling (especially by the expression for the CTR Jacobian matrix) applying beam mechanics to describe cannula shape [10], [11]. Control of continuum robots is challenging in comparison to that of traditional robots whose links are relatively rigid and whose joints are discrete [7], especially for CTR due to the phenomena like torsion, friction, shear, and non-linear constitutive behaviour.

Real-time and accurate control of a CTR can be ensured using an image-guided strategy usually called visual servoing control or vision-based control [11]. In fact, image-guided control enables interventional procedures with high accuracy and interesting medical outcomes due to integration of medical imaging with the surgical workflow. Several related works were proposed in the literature in which the integration of the vision feedback on the control scheme improves considerably the surgical procedures, especially in terms of accuracy and versatility. Different image modalities were used to close the loop mainly using white light images [11], but not only, ultrasounds (US) [12], [13] , magnetic resonance imaging (MRI) [14], and computed tomography [15]. have been investigated as external sensor to control a robotic system, this in a large number of medical and surgical applications. Some medical imaging modalities offer more than just an indirect (intracorporeal) visualization of organs/tissues but an effective means for establishing a reliable diagnosis. Thanks to the recent advances in fiber-optics, light sources and detectors allow performing cellular level, non-invasive and real-time examination of suspected organs/tissues. This procedure is usually called "*optical biopsy*" in opposition to the conventional *"surgical biopsy"* which requires tissue removal, transport and storage for histopathological examination.

The most promising optical biopsy technique is certainly the optical coherence tomography (OCT). OCT is operating under the principle of low coherence interferometry providing very interesting lateral and axial resolutions: 4μm and 3μm, respectively. Depending on the intended use, OCT offers three types of optical biopsies 1D (optical core), 2D (B-Scan image) and 3D (volume). OCT imaging modality is able to reach higher penetration depths 1-5mm compared to only 250μm provided by the confocal microscopy devices. OCT was firstly applied in ophthalmology due to the transparent nature of eyes, their minimal scattering and high light penetration. However, imaging of non-translucent mediums has been performed using longer wavelengths (near infrared) allowing new applications, such as dermatology, cardiology, etc. Since the OCT systems are fiber-optic based principles, it becomes possible to be easily integrated in endoscopic systems for visualizing internal organs. OCT has also been used to perform an ophthalmic surgery [16] and a repetitive biopsy through robot control [17], [18]. As reminder, the CTR have a free axial part, it is in fact possible to slide a fiber-based OCT inside the CTR. It is then advantageous to consider the use of OCT images to perform an optical biopsy and at the same time as an external sensor allowing the position control of the robotic system.

The aim of this paper is to perform OCT image-based in-plane positioning task of CTR with respect to a biological

All authors are with FEMTO-ST Institute, AS2M department, Univ. Bourgogne Franche-Comté/CNRS/ENSMM, 24 rue Savary, 25000 Besançon, France. name.surname@femto-st.fr

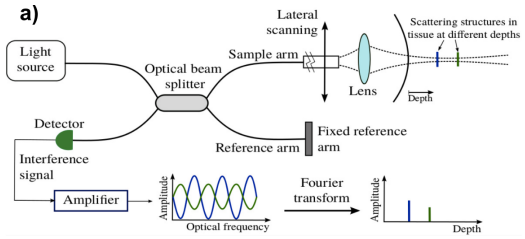

Fig. 1. Principle of the spectral-domain OCT system.

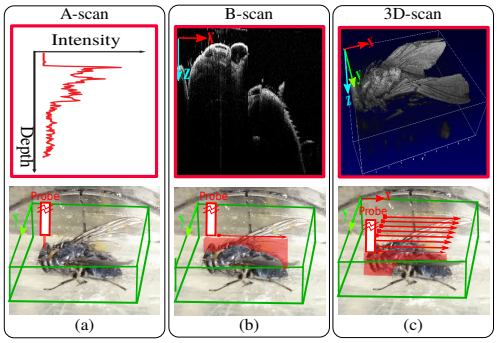

Fig. 2. Illustration of OCT system functioning on its three modes. (a) is an A-Scan optical core, (b) is called B-Scan (2D OCT image) which is the sum of several A-Scan measurements grabbed along one scanning direction, and (c) represents a 3D (volume) OCT image which is obtained by a two-directions scan of the sample.

sample. To do this, we use the B-Scan OCT images for both the optical biopsy acquisition and the control of the CTR tip. The OCT probe views simultaneously the robot tip and the cross-section of the biological sample. In this work, the CTR is considered such as a puncture needle which must reach, with high accuracy, the optical biopsy site (inside the biological sample). Indeed, the human operator (e.g., a physician) defines the suspected area on the sample and the CTR must moves automatically to the target thanks to an image-guided closed-loop controller. To our knowledge, a such investigation, i.e., controlling a CTR using OCT images as signal input on the control loop, has not been reported in the literature yet. The preliminary experimental validation of the developed OCT-based control law on a lab-made CTR has demonstrated encouraging results, especially in term of accuracy.

The paper is organized as follow: Section II deals with a description of the operating of an OCT imaging system. Section III introduces the CTR working principle and the developed CTR. Section IV describes an OCT-based control law using a differential kinematics while the experimental validation of the proposed materials is discussed in Section V. Finally, Section VI concludes the paper and discusses perspectives.

II. OCT Imaging System

As mentioned in the introduction, OCT is an emerging technology for performing high-resolution, cross-sectional, tomographic imaging in real time. OCT system operating is based on a low coherence interferometric technique, usually using near infrared light [19]. In fact, OCT images are obtained by the measure of the reverberate time delay and the intensity of the back-scattered light from the viewed object that gives data about the different scrambling layers of the tissue. From this point of view, it can be noticed that there is a similarity between OCT functioning and that of the ultrasound (US) system in which the laser source is replaced by an ultrasound one. However, since light travels faster than sound (3×10^8 m/s for the light *versus* 1500 m/s for the sound in water), direct measurement of the echo time as in ultrasound systems is not possible. In opposition, in OCT systems this measure is indirectly achieved by using low-coherence interferometry and through a Michelson interferometer (Fig. 1).

Actually, light from a low coherence source is split into reference and sample arm. In the first arm, the lighting rays are reflected by a mirror, when in the second arm, the rays are focused on the sample through different objective lenses. Then, the back-scattered light from the sample interferes with the light returning from the reference arm. Therefore, the resulting signal is revealed by a photo-detector and sent to the signal processing unit. For instance, in Time-Domain OCT (TD-OCT), this is achieved by scanning the reference mirror in aim to grab the signals resulting from all the sample layers, whereas in Fourier-Domain OCT (FD-OCT), the system is fixed recording the spectral interference pattern. The depth reflectivity profile (optical core) of the sample at the focal spot (Fig. 2(a)) is then obtained through a Fourier transform of the grabbed spectral signal. Moving the focused beam across the sample in a straight line generate 2D cross-sectional B-Scan image (Fig. 2(a)) which is the concatenation of A-Scans (Fig. 2(a)) while the concatenation of the B-Scans sections provides a 3D OCT image (Fig. 2(c)).

With respect to US device, OCT does not need any transduction medium or direct contact with the tissues for propagating the lighting rays. The OCT images resolution (depending on the used lighting source wave-length) is requiring micrometer resolution and millimeter penetration depth while US images offer a millimetric resolution (up to the tenth of millimeter) with several centimeters of depth. Due the numerous advantages of the OCT, it is considered as *"optical biopsy"*, in various medical fields, which can be a substitute of the conventional *"physical biopsy"* (Fig. 3).

III. Concentric Tube Robot Description

A CTR is composed of two main parts: the actuator unit and the backbone. The last one is obtained by the assembly of superplastic tubes in a telescopic manner. The backbone is divided in m links where each one is defined by the number of tubes, the resultant curvature κ_j ($j \in 1...m$), and the link length ℓ_j with constant piecewise curvature assumption [6]. A CTR with 3 tubes is usually proposed to obtain 6 degrees of freedom [3], [4] while the actuator space is defined by $\mathbf{q}=[\alpha_1, \rho_1, \alpha_2, \rho_2, \alpha_3, \rho_3,]^\top$ (Fig. 4) and the robot pose is ${}^0\mathbf{T_3}$.

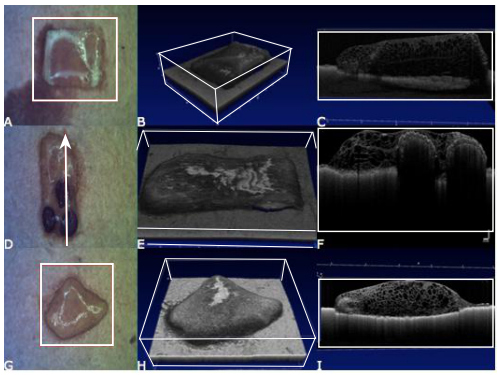

Fig. 3. OCT images of samples of cucumber (A,B,C), kiwi (D,E,F) and grape (G,H,I): (A,D,G) are white light camera image of the sample, white box/line indicates the scanning region; (B,E,H) are volume rendering reconstructed from all the scans; and (C,F,G) are B-scans of a single slice of the sample.

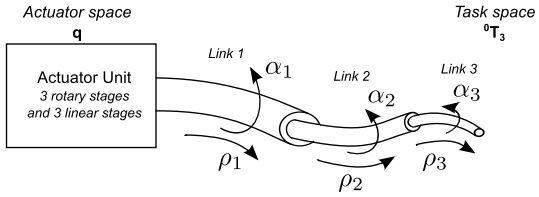

Fig. 4. Working principle of CTR with 3 curved tubes.

In the following, a model-less control is studied while the description of the developed prototype is discussed. It has been designed and used in order to validate the OCT-based control scheme. It is equipped with an actuation unit with 3 linear stages (LIMES 90-55-HSM, step motor with a positioning accuracy $< 16\mu$m) and 3 rotary stages (DRMT 65-D25-HSM, step motor with a repeatability $< 0.02°$) from OWIS GmbH. Each tube is fixed with a mechanical part at the open aperture of the rotary stage which is mounted on the linear stage. It is controlled through a MATLAB implementation on a desktop computer (a Dell Optiplex 7010 with a Intel Core TM 3.4GHz processor).

The tubes which constitute the CTR mechanism were acquired in a straight shape from Euroflex GmbH. The curvature setting is lab-made using a mold and the specimens were placed in an air furnace at ~ 500°C for 20 min and then quenched in water. The tubes geometrical features are listed in Table I. Finally, the developed experimental setup is shown in Fig. 5 where one can see a capillary fiber (with a diameter of 240μm) mounted on the end-effector in order to simulate for example a puncture needle or a surgical instrument.

TABLE I

GEOMETRICAL PARAMETERS OF THE TUBES ASSEMBLED ON THE PROTOTYPE.

Tube i	Tube 1	Tube 2	Tube 3
Curvatures κ_i (m^{-1})	4.91	7.2	9.76
Lengths L_i (m)	0.12	0.155	0.2
Outer diameters (mm)	3.112	2.032	1.32
Wall thickness (mm)	0.222	0.279	0.180
Transmission lengths (mm)	0	200±50	400±50

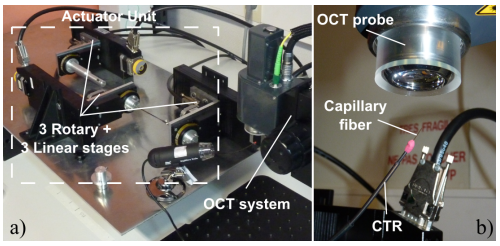

Fig. 5. a) The developed CTR prototype with 3 curved tubes and the OCT system, b) zoom on the capillary fiber and the OCT probe positioned in an *eye-to-hand* configuration.

***Remark 1**: Despite very accurate description of position and orientation, it still very difficult to estimate analytically the CTR robot Jacobian considering torsion and friction since forward kinematics consists of differential equations coupled with boundary conditions [7], [20]. Thereby, generally the Jacobian matrix* $\mathbf{J}$ *is computed through a numerical estimation instead of analytical one. In our case, we want to control the CTR on the image frame. Thus, we will use only two tubes with 2 DOF (α_3, ρ_2=ρ_3), and hold the rest constant (ρ_1, α_1, α_2). Thereby it reduces* $\mathbf{J}$ *to a 2 by 2 square matrix. To computed* $\mathbf{J}$*, we move the robot according to the robot actuators (in our case α_3, ρ_3=ρ_2). Thus, the robot tip position, expressed in the OCT image frame, is computed (using image processing). Several series were carried out in order to optimize the estimation. This approach is sufficient because of the small robot motion needed in case of optical biopsy acquisition (the OCT field-of-view is only 3mm $\times$ 3.54mm) and allows controlling the CTR without using model or additional external sensor.*

IV. OCT-BASED CONTROL LAW USING A DIFFERENTIAL KINEMATICS

A. Basics of Visual Servoing

According to [21], a visual servoing control law aims the control of the robot's motion allowing to make a set of visual features $\mathbf{s}$ ($\mathbf{s} \in \mathbb{R}^k$), which defines the current robot pose $\mathbf{s} = \mathbf{s}\big(\mathbf{x}(t)\big)$ $\big(\mathbf{x}(t) \in SE(3)\big)$, to reach a set of desired features $\mathbf{s}^*$ ($\mathbf{s}^* \in \mathbb{R}^k$), this by minimizing an positioning error given by

$$\mathbf{e} = \mathbf{s}\big(\mathbf{x}(t)\big) - \mathbf{s}^* \tag{1}$$

where $\mathbf{s}$ defines the image coordinates of the capillary fiber.

Note that the time-derivation of $\mathbf{s}$ allows linking the visual features velocity to those of the camera (OCT system) $\mathbf{v}_c \in SE(3)$ $\big(\mathbf{v}_c = [v_x, v_y, v_z, \omega_x, \omega_y, \omega_z]^\top\big)$, more precisely v_i is the instantaneous linear velocity of the origin of the camera frame and ω_i the instantaneous angular velocity of the camera frame. This relationship is defined as follows

$$\dot{\mathbf{s}} = \mathbf{L}_\mathbf{s}\mathbf{v}_c \tag{2}$$

where $\mathbf{L}_\mathbf{s} \in \mathbb{R}^{k\times 6}$ is called *interaction matrix*.

The combination of (1) and (2) allows relating the time-variation of the error $\dot{\mathbf{e}}$ to the robot motion as

$$\dot{\mathbf{e}} = \mathbf{C}\mathbf{L}_\mathbf{s}\mathbf{v}_c \tag{3}$$

Now, applying an exponential decay of the error, we get the following visual controller expression

$$\mathbf{v}_c = -\lambda \widehat{\mathbf{L}_\mathbf{s}^+} \big(\mathbf{s}(t) - \mathbf{s}^*\big) \tag{4}$$

where λ is a positive gain and $\widehat{\mathbf{L}_\mathbf{s}^+}$ is the *Moore-Penrose* pseudo-inverse of the interaction matrix $\mathbf{L_s}$ estimated as follows [21],

$$\mathbf{L_s} = \begin{pmatrix} \frac{-1}{Z} & 0 & \frac{x}{Z} & xy & -(1+x^2) & y \\ 0 & \frac{-1}{Z} & \frac{y}{Z} & 1+y^2 & -xy & -x \end{pmatrix} \tag{5}$$

Z is the depth of the point relative to the camera frame. Note that, in this study, we choose to fix $\widehat{\mathbf{L}_\mathbf{s}}$ to be the interaction matrix ${\mathbf{L}_\mathbf{s}}^*$ obtained at the desired position of the visual sensor as it is often done.

B. Control Law

Our system OCT-robot (Fig. 5) is designed in an *eye-to-hand* configuration. Thus, the relation between the robot velocity $\dot{\mathbf{q}}$ (the joint space of the CTR robot are noticed as $\mathbf{q} = [\alpha_1, \rho_1, \alpha_2, \rho_2, \alpha_3, \rho_3]^\top$) and the camera one $\mathbf{v}_c$ is

$$\dot{\mathbf{q}} = -\mathbf{J}^{-1}(\mathbf{q}) {}^e\mathbf{M}_o \, {}^o\mathbf{M}_c \mathbf{v}_c \tag{6}$$

where $\mathbf{J}^{-1}(\mathbf{q})$ is the robot inverse kinematics Jacobian expressed into the robot tip frame $\mathcal{R}_e$, ${}^e\mathbf{M}_o$ is the twist transformation matrix from the robot base frame $\mathcal{R}_o$ to the end effector frame $\mathcal{R}_e$, and ${}^o\mathbf{M}_c$ is the twist transformation matrix from the camera frame $\mathcal{R}_c$ to the robot base frame $\mathcal{R}_o$. The latter two are of the form

$${}^b\mathbf{M}_a = \begin{bmatrix} {}^b\mathbf{R}_a & [{}^b\mathbf{t}_a]_\wedge \, {}^b\mathbf{R}_a \\ 0_{3\times 3} & {}^b\mathbf{R}_a \end{bmatrix} \tag{7}$$

where ${}^b\mathbf{R}_a$ is the 3×3 rotation matrix from the $\mathcal{R}_a$ to $\mathcal{R}_b$ frames, ${}^b\mathbf{t}_a$ is the 3×1 associated translation, and "$[\ .\ ]_\wedge$" is the skew symmetric matrix associated to the cross-product.

C. Visual Features Tracking in OCT Images

Probably, the more challenging task in an OCT-based visual servoing process is the ability to extract and track over time visual features, especially when it concerns the visualization of a biological sample. It can be highlighted that OCT images are characterized by a high image noise (e.g., weak signal to noise ratio) and a low texture. Consequently, the visual tracking of the current visual features **s***(t)* becomes difficult. However, due the fact that this paper deals mainly with the control of a CTR mechanism using the OCT images as signal inputs in the control loop, we have chosen to minimize the image processing task. Thus, to tackle this problem of tracking, we implement a conventional normalized cross-correlation (NCC) [22] method to follow over time the robot tip in the OCT images (Fig. 6). The NCC expression is given by

$$NCC = \frac{\sum_{x,y} \big(I(x,y) - \bar{I}\big)\big(t(x-u, y-v) - \bar{t}\big)}{\Big(\sum_{x,y} \big(I(x,y) - \bar{I}\big)^2 \sum_{x,y} \big(t(x-u, y-v) - \bar{t}\big)^2\Big)^{\frac{1}{2}}} \tag{8}$$

where $I(x,y)$ is the OCT image, $\bar{I}$ the mean of I, t is the correlation template feature and $\bar{t}$ its mean, and (u,v) defines template t coordinates center.

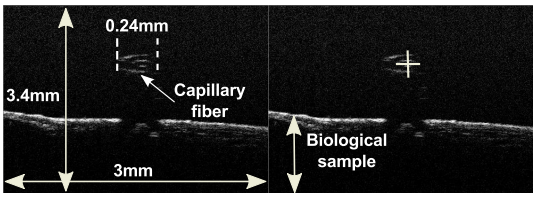

Fig. 6. Tracking of the end-effector based on correlation: a) 2D OCT image (500 × 350 pixels) and b) the tracked position of the end-effector positioned above the biological sample.

Furthermore, the image processing processes were performed using the open-source library OpenCV which is integrated into our open-source lab-made library cvLink [1] (operating under the MATLAB SIMULINK framework).

Finally, Fig. 7 depicts the global block diagram which summarizes the different followed steps of the proposed OCT-based visual servoing control law for CTR purposes in case of optical biopsy acquisition and positioning.

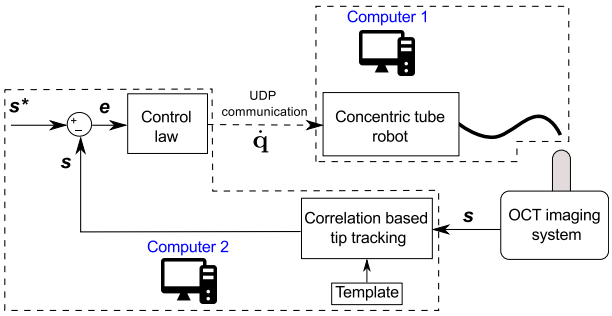

Fig. 7. Block diagram for the complete OCT-based control scheme.

V. EXPERIMENTAL VALIDATION

A. Experimental Setup

For the experimental validation, the previously described prototype (Section III) is used and controlled with computer 1 in Fig. 7. The second computer, a Dell Optiplex 7010 with a Intel Core TM 3.4GHz processor named computer 2 in Fig. 7, is exclusively dedicated to the OCT images grabbing and image processing algorithms running. Both computers communicate asynchronously using an UDP protocol.

The whole system (Fig.5) was mounted in an *eye-to-hand* configuration. This means that the OCT imaging system (a Telesto-II 1300nm from THORLABS) is placed upper the robot tip as well as the biological sample. This configuration allows a simultaneous visualization of the robot tip and the biological sample. The considered OCT images are B-scan slices (acquired in the xy plane) having a resolution of 500 × 350 pixels grabbed under a frame-rate up to 25 frames per second.

In practical implementation, the control law processes the variation of the robot actuator $\delta\mathbf{q}$ in order to reach the fixed tolerance threshold ξ and it is stopped when $\mathbf{e} \leq \xi$.

[1] https://sourcesup.renater.fr/cvlink/

B. 1 DOF validation

In order to validate the proposed control scheme, the CTR is positioned on the OCT field of view. Afterwards, the operator chooses the B-scan where he wants to perform the positioning of the capillary fiber. The next step is to point out the desired position $\mathbf{s}^*$ with mouse double clicking on the image. The results of the positioning along X and Y are respectively shown in Fig. 8 and Fig. 9.

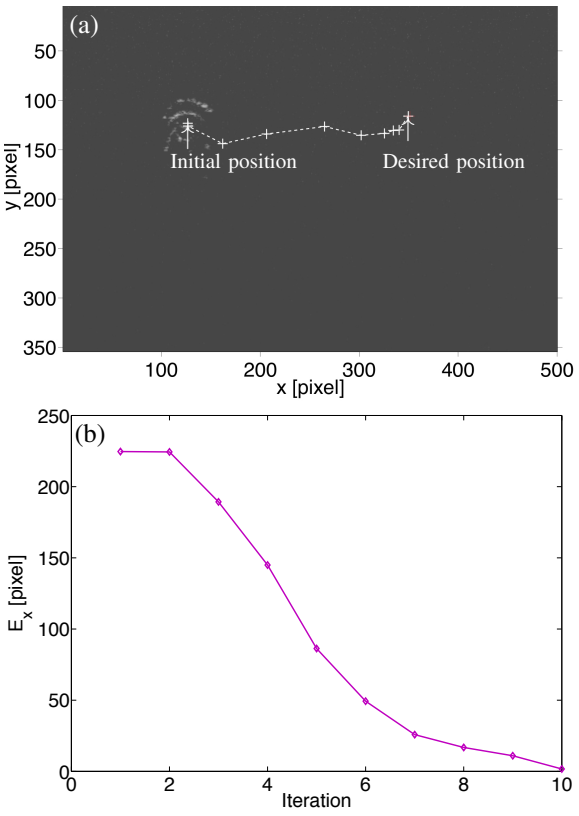

Fig. 8. 1D positioning: (a) along X with λ=0.05, ξ=60 μm and (b) the evolution of the error $\mathbf{e}$ for 10 iterations.

As can be seen in Fig. 8-(a), the end-effector position $\mathbf{s}(t)$ converged to the desired position $\mathbf{s}^*$. The movement is stopped when the error $\mathbf{e}(t)$ is less than the fixed tolerance threshold ξ=60 μm during this test. The position error is about 10 μm ($\sim$ 1.67 pixels in Fig. 8-(b)) after 10 iterations.

Along Y, the convergence is shown in Fig. 9-(a) and the evolution of the robot tip is observed in Fig. 9-(a) with the final error about 79 μm ($\sim$ 7.9 pixels *cf.* Fig. 9-(b), ξ=100 μm) after 23 iterations.

Afterwards, the effect of controller parameters (λ and ξ) is studied in order to assess the high accuracy positioning ability of the proposed OCT-based CTR control. The results are summed up in Table II where one can see a final position error up to 10μm along X and 74μm along Y. The iteration number can be reduced by increasing the controller gain thus its value will be fixed according to the application constraints. These values are up to now the lowest positioning error obtained in closed loop control of CTR.

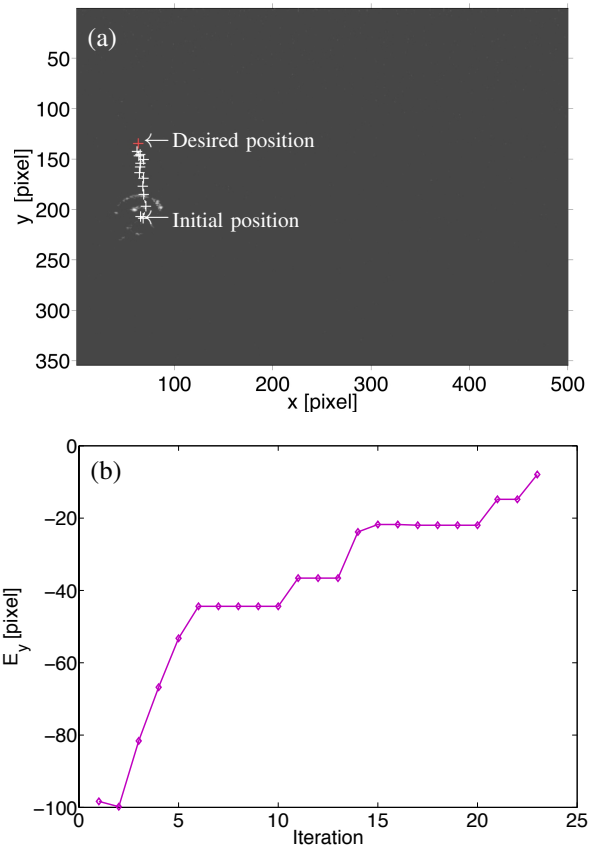

Fig. 9. 1D positioning: (a) along Y λ=0.2, ξ=100 μm and (b) the evolution of the error $\mathbf{e}$ for 23 iterations.

TABLE II

PERFORMANCE ANALYSIS ACCORDING TO THE CONTROL LAW PARAMETERS.

Controller parameters	Iteration count	Final position error (μm)
Along X		
λ=0.01, ξ=240 μm	22	210 μm
λ=0.05, ξ=60 μm	10	10 μm
λ=0.1, ξ=60 μm	6	12 μm
Along Y		
λ=0.05, ξ=300 μm	18	290 μm
λ=0.2, ξ=100 μm	23	79 μm
λ=0.3, ξ=100 μm	7	74 μm

C. 2 DOF validation

A 2D control was also performed in order to validate the proposed control scheme. The previously described procedure is applied again.

The final position error is measuring about 295μm during the test presented in Fig. 10. It can be reduced by varying λ and ξ following the trend observed in Table II. A position error about 55μm is obtained for λ=0.1 and ξ=100μm. One can observe that the path to the desired position is not in straight line. This can be explained by the coefficients of the estimated jacobian where the actuation of α_3 generates

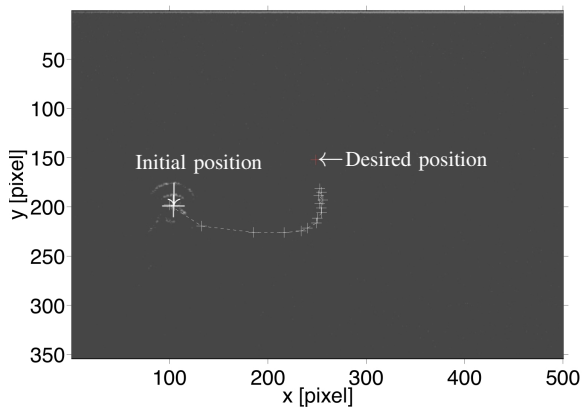

Fig. 10. 2D positioning with λ=0.1, ξ=300 μm, and iteration=19.

large movement along X and Y compared to ρ_3=ρ_2 effect. In addition, differential kinematics based control of CTR has shown a non linear path to the desired position as previously observed in [11]. This behavior could be explained by the friction and the torsion observed with the amplitude of the considered displacement.

VI. Conclusion

In this paper were presented preliminary results on OCT-based control of CTR which are to our knowledge not presented in the literature yet. The OCT imaging system is described and its ability for optical biopsy is highlighted. Afterwards, the developed CTR prototype is briefly introduced. A control law based on OCT images is introduced which has two main advantages: the visual features tracking is based on a conventional normalized cross-correlation (NCC) and it is model-less control because the robot jacobian matrix is numerically estimated. The proposed control scheme is experimentally validated with tests in 1D (successively along X and Y) and 2D. It was demonstrated that OCT-based control of CTR enables to achieve high accuracy positioning task (up to 10μm position error). These results are clearly another confirmation of the CTR ability to be versatile and once again confirm its *Swiss Army knife* role in robot-assisted interventions. Future works will be focused on the extension of the proposed control law to more than 2D positioning task. The challenges will be on the development of surgical tools visible under OCT imaging system using high resolution additive manufacturing technologies.

Acknowledgment

This work is conducted with a financial support from the project NEMRO (ANR-14-CE17-0013-01) funded by the ANR and the financial support of the Franche-Comté région (FRANCHIR), France. It is also performed in the framework of the Labex ACTION (ANR-11-LABEX-01-001).

References

[1] R. H. Taylor, A. Menciassi, G. Fichtinger, and P. Dario, "Medical robotics and computer-integrated surgery," in *Springer handbook of robotics*. Springer, 2008, pp. 1199–1222.

[2] J. Burgner-Kahrs, D. C. Rucker, and H. Choset, "Continuum robots for medical applications: A survey," *IEEE Trans. on Robotics*, vol. 31, no. 6, pp. 1261–1280, 2015.

[3] M. T. Chikhaoui, K. Rabenorosoa, and N. Andreff, "Kinematics and performance analysis of a novel concentric tube robotic structure with embedded soft micro-actuation," *Mechanism and Machine Theory*, vol. 104, pp. 234–254, 2016.

[4] Z. Li, L. Wu, H. Ren, and H. Yu, "Kinematic comparison of surgical tendon-driven manipulators and concentric tube manipulators," *Mechanism and Machine Theory*, vol. 107, pp. 148–165, 2017.

[5] P. E. Dupont, J. Lock, B. Itkowitz, and E. Butler, "Design and control of concentric-tube robots," *IEEE Trans. on Robotics*, vol. 26, pp. 209–225, 2010.

[6] I. R. J. Webster and B. A. Jones, "Design and kinematic modeling of constant curvature continuum robots: A review," *Int. J. of Robotics Research*, vol. 29, pp. 1661–1683, 2010.

[7] H. B. Gilbert, D. C. Rucker, and R. J. Webster III, "Concentric tube robots: The state of the art and future directions," in *Robotics Research*. Springer, 2016, pp. 253–269.

[8] C. Bergeles, A. Gosline, N. Vasilyev, P. Codd, P. del Nido, and P. Dupont, "Concentric tube robot design and optimization based on task and anatomical constraints," *IEEE Trans. on Robotics*, vol. 31, no. 1, pp. 67–84, Feb 2015.

[9] C. Girerd, K. Rabenorosoa, and P. Renaud, "Combining tube design and simple kinematic strategy for follow-the-leader deployment of concentric-tube robots," in *Advances in Robot Kinematics*, 2016.

[10] R. Xu, A. Asadian, A. S. Naidu, and R. V. Patel, "Position control of concentric-tube continuum robots using a modified jacobian-based approach," in *IEEE Int. Conf. Robotics and Automation on*. 2013, pp. 5813–5818.

[11] R. J. Webster III, J. P. Swensen, J. M. Romano, and N. J. Cowan, "Closed-form differential kinematics for concentric-tube continuum robots with application to visual servoing," in *Experimental Robotics*. Springer, 2009, pp. 485–494.

[12] C. Nadeau, H. Ren, A. Krupa, and P. Dupont, "Intensity-based visual servoing for instrument and tissue tracking in 3d ultrasound volumes," *IEEE Trans. on Automation Science and Engineering*, vol. 12, no. 1, pp. 367–371, 2015.

[13] M. Ourak, B. Tamadazte, O. Lehmann and N. Andreff, "Wavelets-based 6 DOF visual servoing, "IEEE Int. Conf. on Robotics and Automation", Stockholm, 2016, pp. 3414-3419.

[14] H. Su, D. C. Cardona, W. Shang, A. Camilo, G. A. Cole, D. C. Rucker, R. J. Webster, and G. S. Fischer, "A mri-guided concentric tube continuum robot with piezoelectric actuation: a feasibility study," in *IEEE Int. Conf. on Robotics and Automation*. 2012, pp. 1939–1945.

[15] I. S. Godage, A. A. Remirez, R. Wirz, K. D. Weaver, J. Burgner-Kahrs, and R. J. Webster, "Robotic intracerebral hemorrhage evacuation: An in-scanner approach with concentric tube robots," in *IEEE/RSJ Int. Conf. on Intelligent Robots and Systems*. IEEE, 2015, pp. 1447–1452.

[16] H. Yu, J.-H. Shen, K. M. Joos, and N. Simaan, "Calibration and integration of b-mode optical coherence tomography for assistive control in robotic microsurgery," *IEEE/ASME Trans. on Mechatronics*, vol. 21, no. 6, pp. 2613–2623, 2016.

[17] M. Ourak, B. Tamadazte, and N. Andreff, "Partitioned camera-OCT based 6 dof visual servoing for automatic repetitive optical biopsies," in *IEEE/RSJ Int. Conf. on Intelligent Robots and Systems,*. 2016, pp. 2337–2342.

[18] M. Ourak, A. De Simone, B. Tamadazte, G. J. Laurent, A. Menciassi and N. Andreff, "Automated in-plane OCT-probe positioning towards repetitive optical biopsies," IEEE Int. Conf. on Robotics and Automation, Stockholm, 2016, pp. 4186-4191.

[19] D. Huang, E. A. Swanson, C. P. Lin, J. S. Schuman, W. G. Stinson, W. Chang, M. R. Hee, T. Flotte, K. Gregory, C. A. Puliafito *et al.*, "Optical coherence tomography," *Science (New York, NY)*, vol. 254, no. 5035, p. 1178, 1991.

[20] P. E. Dupont, J. Lock, and E. Butler, "Torsional kinematic model for concentric tube robots," in *IEEE Int. Conf. on Robotics and Automation*, 2009.

[21] F. Chaumette and S. Hutchinson, "Visual servo control. i. basic approaches," *IEEE Robotics & Automation Magazine*, vol. 13, no. 4, pp. 82–90, 2006.

[22] D. Forsyth and J. Ponce, Eds., *Computer Vision A Modern Approach*. Pearson, 2012.